Capillary cohesion of different granular materials determined from uniaxial compression and water retention tests

Dennis Heinrich[1*], *Marius* Milatz[1]

[1]Hamburg University of Technology, Institute of Geotechnical Engineering and Construction Management, 21079 Hamburg, Germany

Abstract. In this conference contribution, we present and discuss the results for capillary cohesion of different granular materials determined through different approaches. First, we consider macroscopic uniaxial compression tests with varying degrees of saturation. Second, we derive theoretical capillary cohesion from the water retention curve (WRC) measured in macroscopic water retention experiments. Finally, capillary cohesion is calculated from air-water interfacial areas and solid-water interfacial areas extracted from CT images acquired during a cyclic water retention experiment. An attempt is made to link the macroscopic results of capillary cohesion based on microscopic insights from CT imaging experiments.

1 Introduction

Granular soils are generally considered cohesionless and tend to fall apart due to gravity in the dry or saturated state because of a lack of *present* cohesion. However, as a result of capillary effects in the unsaturated state, the grain skeleton can transfer external loads as matric suction attracts particles to each other, leading to a certain amount of shear strength. *E. g.,* the effect of matric suction in granular soils is visible when sculpting sand or considering its compactibility. A measure of shear strength of unsaturated soils is either the *capillary /apparent* cohesion or suction stress, as proposed by [1]. Capillary cohesion from uniaxial compression tests, on the one hand, can be calculated based on Mohr-Coulomb's yield criterion following [2] as

$$c_\mathrm{c} = 0.5\,\sigma_\mathrm{max}(\cos\varphi' - (1-\sin\varphi')\cdot\tan\varphi'), \tag{1}$$

where σ_max denotes uniaxial compressive strength (given as the maximum transmissible stress) and φ' is the effective friction angle, *e. g.*, gained from triaxial tests. Suction stress, on the other hand, describes the impact of capillary effects on the effective stress and can be described by the following equation as

$$\sigma_\mathrm{s} = S_\mathrm{e}\,s + \Sigma_\mathrm{i}\gamma_\mathrm{i}\frac{\delta A_\mathrm{i}}{\delta V}, \tag{2}$$

with S_e being the effective degree of saturation, s the matric suction, γ_i the surface energies of different interfaces and $A_\mathrm{i}/V_\mathrm{i}$ the corresponding volume averaged (specific) interfacial areas [3]. Different authors have already proposed a formulation of effective stress in unsaturated soils based on interfacial areas such as [4–6]. Based on that, the equation for suction stress is further modified, as proposed by [7], to calculate suction stress directly from interfacial areas as

$$\sigma_\mathrm{s} = \frac{a^\mathrm{sw}}{a^\mathrm{s}}\gamma H + \gamma a^\mathrm{nw}, \tag{3}$$

with γ describing the surface tension of water at 20°C, a^s being the volume averaged (specific) solid surface area and H being the mean curvature of the air-water interfacial area and a^sw and a^nw representing the specific solid-water and air-water interfacial area.

By application of 4D (3D+time) *in situ* computed tomography (CT) imaging experiments, microscopic *capillary state variables,* such as interfacial areas (air to water, solid to water), and others, like contact angles, coordination numbers and others, can be evaluated from the resulting volumetric image data, *e. g.,* see [8].

In this study, we present different approaches to determine capillary cohesion and to present a link from microscopic *capillary state variables* to macroscopic capillary cohesion.

2 Materials and methods

2.1 Materials and specimen preparation

The materials tested in the presented experiments, displayed in Table 1, can be split into two groups: One group being quasi-monodisperse particles consisting of soda-lime glass beads, the other group being polydisperse particle packings.

Table 1: Tested materials. Given are the grain density ρ_s, the void ratios e_min and e_max and the effective friction angle φ'.

Group/Name	ρ_s $\left(\frac{\mathrm{g}}{\mathrm{cm}^3}\right)$	e_min (–)	e_max (–)	φ' (°)
Polydisperse				
Hamburg Sand	2.64	0.520	0.805	38.2
Hamburg Glass	2.50	0.550	0.672	23.9

* Corresponding author: dennis.heinrich@tuhh.de

Quasi-monodisperse glass beads				
d = 1.000±0.050 mm	2.50	0.574	0.648	27.2
d = 0.655±0.055 mm	2.50	0.571	0.677	23.0
d = 0.550±0.050 mm	2.50	0.545	0.681	27.2

The corresponding WRC for each specimen in the range of $0.3 < S_r \leq 1$ can be found in Fig. 1 [9]. All materials can be considered to be hydrophilic due to a contact angle way lower than 90°.

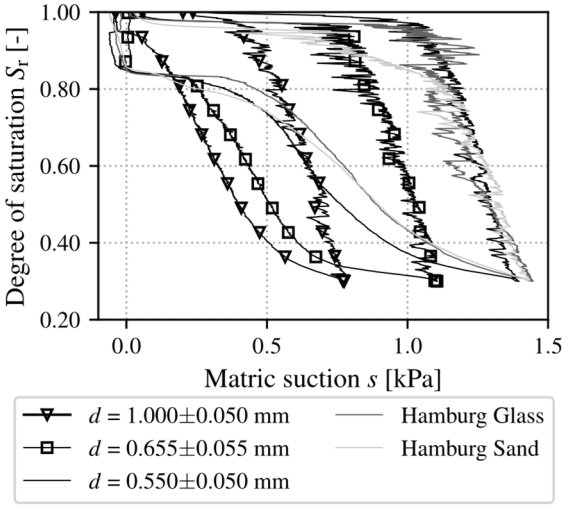

Fig. 1. WRC for each material for initial drainage and first consecutive imbibition path, taken from [9].

2.2 Experimental set-ups

UNSAT-*Pi* We determine the capillary cohesion with the help of a custom-built uniaxial compression device based on a set-up, namely the UNSAT-*Pi,* as depicted in Fig. 2. It's a miniaturised set-up that additionally allows being placed into the chamber of a computer-tomograph. The original set-up is described in [10] and [11].

The uniaxial compression test is a standard soil mechanics test to investigate cohesive soils' uniaxial compression strength and undrained shear strength. It is selected for its ability to apply shear to a soil specimen that is laterally unconfined, i. e. under quasi-zero confining pressure. In unsaturated granular soils, where low matric suction results in capillary cohesion of only a few kilopascals, capillary effects are the dominant factor in the mechanical stress state during this test due to the negligible confinement pressure. Therefore, the uniaxial compression test enables to study the impact of the degree of saturation and matric suction on shear strength without confining pressure superposing the relatively small capillary effects.

Some modifications have been made to the UNSAT-*Pi* to increase its accuracy and reliability. Mainly, the housing was reworked to fit a new load cell of type KD34s manufactured by ME-Meßsysteme GmbH with a full-scale range down to ± 0.25 N. Here, sensors with a full-scale range of ± 1 N and ± 2 N are used. Additionally, a NEMA 17 stepper motor is mounted to drive the loading piston with a resolution of axial displacement of 1.56×10^{-4} mm/step. The new housing is machined from aluminium instead of PVC.

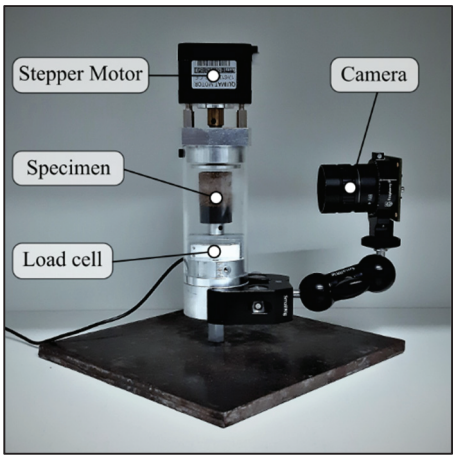

Fig. 2. Modified uniaxial compression set-up as published in [11] with additional camera system for tracking of specimen deformation.

To keep track of the volume change during shearing, we evaluate images of a camera system attached to the set-up capturing the specimen's deformation. The shear strength σ_{max} is calculated based on the assumed circular cross-section A in the centre height of the specimen at the point where the maximum compressive force F_{max} is measured during shearing. With this, compressive strength is calculated as $\sigma_{max} = F_{max}/A$ and capillary cohesion c_c as of Eq. 1, respectively.

To prepare a specimen to be tested via uniaxial compression, water and sand grains are mixed in a bowl and then filled into a mould with a diameter of 20 mm and finally compacted to a specimen height of 20 mm, corresponding to an initial void ratio of $e = 0.61$. Fig. 3 shows a specimen made of Hamburg Sand before and after testing. Compared to cohesive soils, the materials used are coarse-grained so that the water phase in the pores can interact with the ambient air. The test method is, therefore, no longer considered undrained since evaporation is taking place. Also, the specimen preparation leads to water loss, as water can stick to the mixing bowl. All results are presented as S_r determined via oven drying *after* test execution to account for water loss during specimen preparation and evaporation during testing.

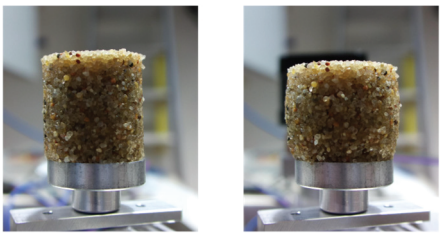

Fig. 3. Specimen made of Hamburg Sand at a degree of saturation $S_r = 0.5$ and an initial void ratio $e_0 = 0.61$ before (left) and after shearing (right) in an uniaxial compression experiment. No membranes are used for stabilization.

UNSAT-*Pi* 2 The interfacial areas discussed in this contribution originate from *in situ* CT images captured during cyclic water retention experiments performed

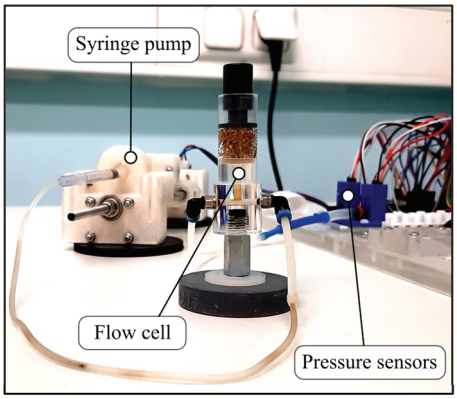

Fig. 4. Measurement set-up showing the flow cell, including a specimen made of Hamburg Sand, a pair of pressure sensors and a syringe pump for control of degree of saturation [13].

with the help of a miniaturised flow cell, namely the UNSAT-*Pi* 2, as shown in Fig. 4 [8]. Here, "cyclic" water retention refers to the testing procedure, where initially water-saturated specimens undergo a first drainage followed by consecutive imbibition.

The set-up follows a tensiometer-based approach for measuring occurring matric suction in response to the change in degree of saturation controlled by the attached syringe pump. Further details regarding the set-up can be taken from [12] and [13].

This set-up is also miniaturized to be placed inside a CT chamber for image acquisition during testing. The material is pluviated into the water filled flow cell and compacted to the desired height. During image acquisition, the flow is stopped. For subsequent image processing, the software product *Avizo* (Thermofisher Scientific Inc.) is used. For identification of interfacial areas, first, the tomographic image dataset needs to be segmented into the three present material phases being air, water and solid. This is based on the *Avizo* module "2D-Histogram Segmentation". Afterwards, the calculation of interfacial areas utilizes the module "Generate Surface". No smoothing was applied when computing interfacial areas. Tomographic data further shows, that beyond the point air entry, within the capillary regime, the water phase is distributed quite homogeneously. Further details are given in [8].

3 Results

In the following, results for capillary cohesion derived from three different experiments are presented: (1) macroscopic uniaxial compression tests on all five materials according to Table 1, (2) macroscopic cyclic water retention experiments on Hamburg Sand and (3) "microscopic" cyclic water retention experiments on Hamburg Sand during *in situ* CT imaging with the extraction of the interfacial areas. In the end, all results for capillary cohesion will be compared.

3.1 Capillary cohesion based on uniaxial compression experiments

The result for capillary cohesion of monodisperse glass bead packings for varying degrees of saturation computed based on Eq. 1 can be seen in Fig. 5. The data

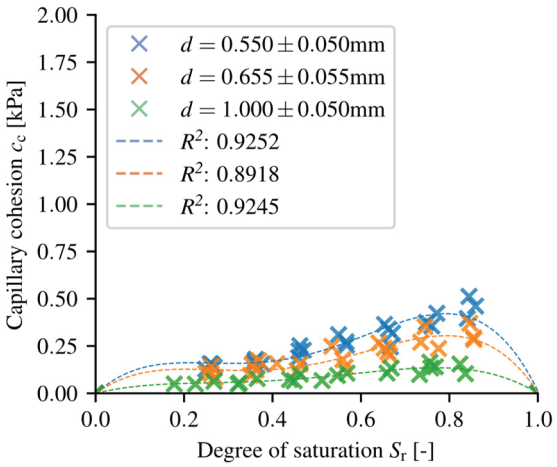

Fig. 5. Scatterplots showing the determined capillary cohesion of monodisperse glass bead specimens at varying degree of saturation and initial void ratio $e_0 = 0.61$. Each point describes an individual sample.

show an increase of capillary cohesion for a decreasing particle diameter. This agrees with the theory of capillarity, *e. g.,* the capillary rise is more dominant in smaller pore spaces. Following [14], who studied the tensile strength dependency on the water content of granular soils, the impact of capillary bridges on tensile strength is more dominant for lower degrees of saturation. In contrast, matric suction is more relevant for higher degrees of saturation. A polynomial fit of fourth order was determined for each material which approximates capillary cohesion as a function of the degree of saturation. A vanishing capillary cohesion is assumed for $S_r = 0$ and $S_r = 1$. The quality of the fitting is represented by the coefficient of determination $R^2 \geq 0.89$.

The results for the two polydisperse materials are shown in Fig. 6. It is noticeable that the determined maximum capillary cohesion of Hamburg Sand on the whole spectrum of S_r is more prominent than for Hamburg Glass and for the monodisperse glass bead specimens and way more scattered. This behaviour is also indicated by the coefficient of determination

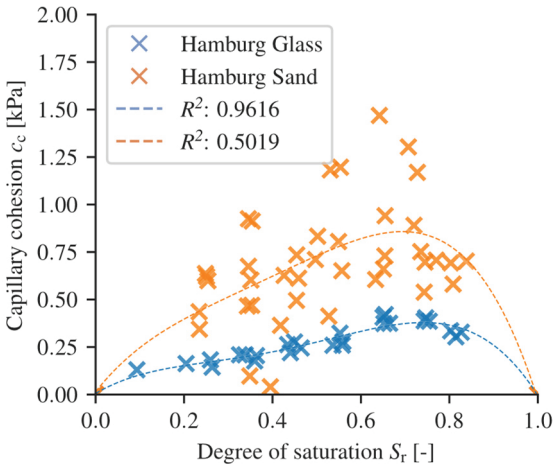

Fig. 6. Scatterplot showing the determined capillary cohesion of polydisperse specimens at varying degree of saturation and initial void ratio $e_0 = 0.61$. Each point describes an individual sample.

$R^2 = 0.5$. An explanation for this behaviour may be found in the less spherical and more edgy shape of the sand grains as compared to the glass beads, leading to grain interlocking effects influencing uniaxial compressive strength and, thus, the derived capillary cohesion. For all materials, the distribution of capillary cohesion shows a peak at higher degrees of saturation, which is in accordance with the findings of [14].

3.2 Capillary cohesion based on the WRC

By neglecting the influence of interfacial areas on the effective stress, which may be valid for the capillary regime [3], see Eq. 2, the suction stress can be directly computed by multiplying the macroscopic measurement of matric suction and degree of saturation from a water retention experiment. Capillary cohesion is then obtained by multiplying suction stress by $\tan\varphi'$ according to Eq. 4

$$c_c = \sigma_s \cdot \tan\varphi' = S_e\, s \cdot \tan\varphi' \,. \tag{4}$$

Here, S_r is used instead of S_e to present the entire course of executed cyclic water retention experiment, see Fig. 7. Starting at the saturated state, the capillary cohesion rapidly increases and peaks at around $S_r = 0.8$, decreases with a lower degree of saturation and eventually vanishes at $S_r = 0$. This behaviour agrees with the results from macroscopic uniaxial compression experiments. Also, the curve shows a dependency of capillary cohesion on the flow direction, *e. g.*, capillary cohesion is higher during drainage compared to imbibition and can therefore be considered hysteretic in theory.

3.3 Capillary cohesion computed from interfacial areas measured in a CT experiment

When preparing this contribution, the interfacial areas and corresponding suction stress calculations are available from an *in situ* CT experiment on Hamburg Sand with cyclic drainage and imbibition using the UNSAT-Pi 2 [8]. The corresponding research data is openly available. This allows for the evaluation of interfacial areas depending on the degree of saturation but neglects the volume change behaviour compared to the experiment during uniaxial loading.

Following [8], the dependency of air-water interfacial area a^{nw} and solid-water interfacial area a^{sw} on the degree of saturation is shown in Fig. 8. The results are based on CT data inside a cubic subvolume with an edge length of 800 px (8 mm) extracted from a full-field scan of the whole Hamburg Sand specimen. The dependency of a^{nw} on S_r shows a peak value at $0.3 < S_r < 0.4$, which follows the findings of [6]. There is no data for lower degrees of saturation, as the measurement of matric suction is based on a tensiometer approach, and the connectivity of the water phase could not be ensured for $S_r < 0.3$. Based on theoretical considerations, a^{nw} disappears in the dry or saturated state. Besides that, a^{sw} will disappear in the dry state and be identical to the solid surface area a^{s} in the saturated state. In between these states, a monotonic rise of a^{sw}can be observed. Also, comparing the scales of both graphs, the more significant influence of the solid-water interfacial area on suction stress as a representation of the active surface of matric suction acting on soil grains becomes clear.

To yield results for σ_s according to Eq. 3, the surface tension γ – taken from literature – is assumed to be 0.07275 N/m. Supplementary to that, the mean curvature H of the air-water interfacial area was determined by evaluating 2D slices of tomographic data on selected capillary bridges for each step of the performed cyclic water retention experiment [8]. The

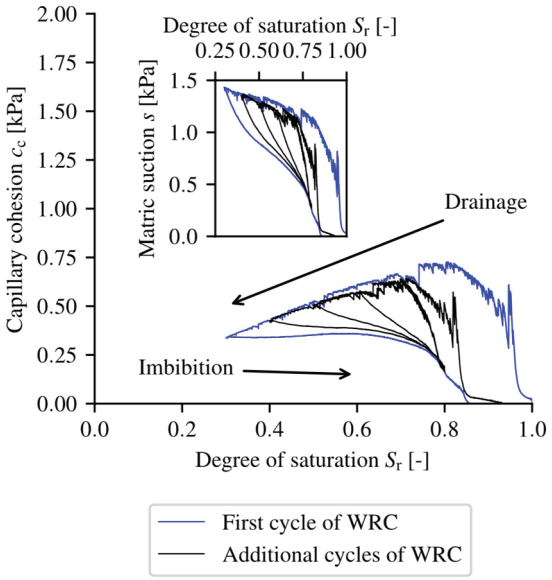

Fig. 7. Capillary cohesion of Hamburg Sand derived from a cyclic water retention curve (inset plot) in dependency on the degree of saturation at a void ratio $e_0 = 0.61$.

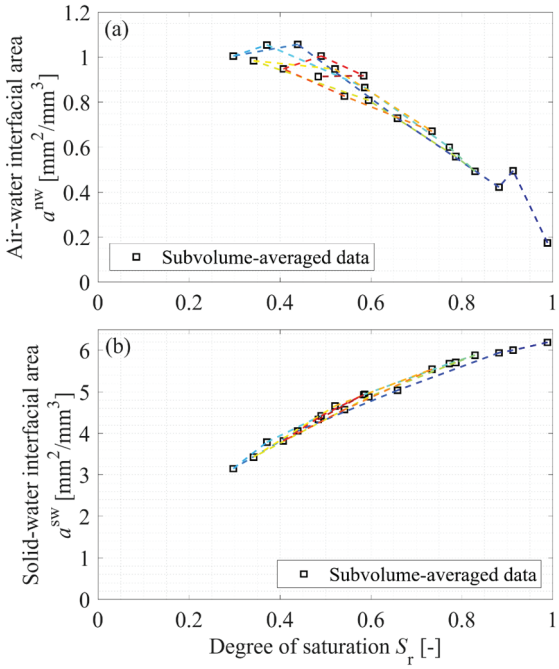

Fig. 8. Dependency of air-water interfacial area (top) and solid-water interfacial area (bottom) on the degree of saturation during cyclic water retention experiments, taken from [8].

definition used for the mean curvature is given by the Young-Laplace equation

$$p_c = \gamma H = \gamma \left(\frac{1}{R_1} + \frac{1}{R_2}\right), \quad (5)$$

with p_c being the capillary pressure (or matric suction) and R_1 and R_2 being the principal radii of curvature of an arbitrarily shaped surface. Only the former radius is used, and the latter is neglected under the assumption of being infinity under 2D conditions [8].

Fig. 9 shows the 2D evolution of the radius of curvature R_1 along the consecutively performed steps of the executed cyclic water retention experiment. A series of measurements for each experimental step was performed on selected capillary bridges, and the mean value for each step was calculated. It can be seen that the radius of curvature tends to rise during imbibition steps and decreases during drainage, respectively.

The evaluation of Eq. 3, considering the results for interfacial areas (Fig. 8), the evolution of radius of curvature (Fig. 9), and the assumed surface tension $\gamma = 0.07275$ N/m yields the suction stress from *in situ* water retention experiments. The conversion of suction stress into capillary cohesion is again computed via Eq. 4, here with $\varphi' = 33.9\,°$ to account for a void ratio $e = 0.65$ and is displayed in Fig. 10. The course of capillary cohesion follows the one of uniaxial compression but with a lower magnitude in areas of a high degree of saturation and a non-existent (or less pronounced) peak value. The behaviour of diminishing capillary cohesion towards the saturated state could be directly obtained from the image data and is found to be plausible.

3.4 Comparison of capillary cohesion determined on the micro and macro scale

Fig. 11 shows a comparison of all discussed approaches for calculating capillary cohesion for Hamburg Sand. The results are all within the same order of magnitude. To emphasise, the capillary cohesion determined in uniaxial compression tests and derived from the WRC has been performed at an initial void ratio $e_0 = 0.61$,

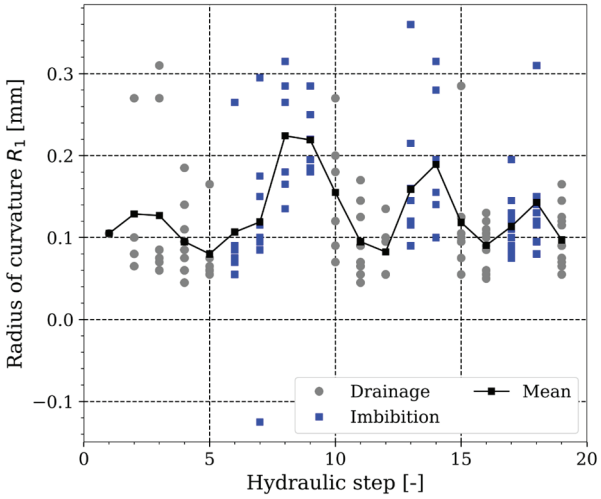

Fig. 9. Evolution of radius of curvature R_1during consecutive drainage and imbibition steps of the performed water retention experiment evaluated on 2D image slices, taken from [8].

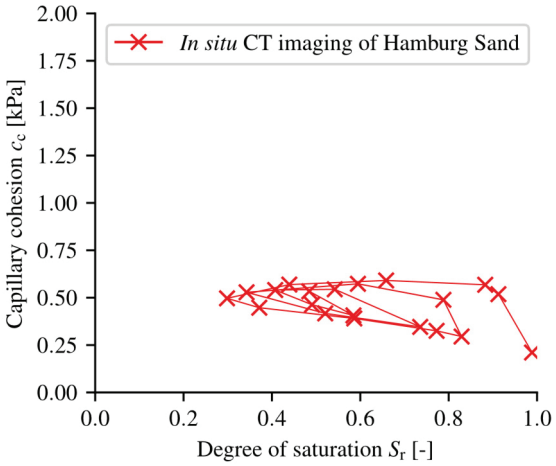

Fig. 10. Capillary cohesion derived from air-water interfacial areas and the solid-water interfacial areas extracted from microscopic *in situ* CT images during a cyclic water retention experiment on Hamburg Sand, starting at $S_r = 1.0$. Each cross marks the acquisition of a CT-image.

whereas the data from *in situ* CT imaging experiments is based on an $e_0 = 0.65$. Interestingly, the curves based on uniaxial compression experiments and derived from the WRC match quite well in the range of $0.8\ S_r \leq 1.0$ and begin to diverge from each other for a lower degree of saturation but still run with a similar gradient. Also, the peak values are shifted.

The course of capillary cohesion derived from interfacial areas based on Eq. 3 and Eq. 4 is lower for $0.55 < S_r \leq 1.0$ but lies within the hysteretic loop based on the theoretical WRC. At $0.3 < S_r \leq 0.55$, capillary cohesion lies approximately in the middle between the uniaxial compression and WRC-based results. For $S_r < 0.3$ no reliable statement can be made.

4 Discussion

Values for maximum tensile strength up to 8.5 kPa for limestone agglomerates are reported by [14]. German construction codes, such as [15], also list capillary cohesion up to 8 kPa for granular soils in general. [6], who studied glass beads with a particle diameter of

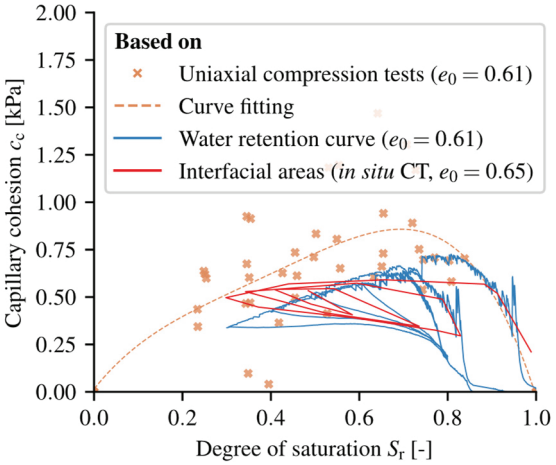

Fig. 11. Capillary cohesion determined on different scales. All results shown are based on experiments using Hamburg Sand.

$0.2\,\text{mm} < d < 0.4\,\text{mm}$ during direct shear testing, identified shear strength of this material up to 1.2 kPa. Considering Eq. 1 and a reported friction angle of $\varphi' \cong 33{,}25\,°$, this shear strength could be translated into capillary cohesion of up to 0.32 kPa. This value for capillary cohesion is lower than the finest glass beads used in this study examined via uniaxial compression.

The magnitude and the course of the resulting capillary cohesion agree with the literature values or at least remain within these limits indicated by the literature and support the general assumption of low capillary cohesion values for granular soils compared to cohesive soils. There are some uncertainties in the evaluation of both the macroscopic uniaxial compression and the microscopic *in situ* water retention experiments that need to be addressed:
On the side of macroscopic uniaxial compression tests, the volume change behaviour, or deformation, cannot be captured, as well as in *in situ* CT experiments focusing on uniaxial compression [16]. It is assumed that the initial void ratios e_0 in our uniaxial compression tests for each tested specimen do not differ noticeably from each other. The influence of changing void ratio during shearing on the capillary cohesion cannot be characterized, but the void ratio at failure is assumed to be increased due to dilatancy. Compared to that, the void ratio during water retention experiments is almost unchanged. Also, the influence of changing flow direction, drainage or imbibition, is only known for the water retention experiments but remains unknown for a specimen under uniaxial load. Due to dilatancy, it is also reasonable to assume that the specimen is on a drainage or at least a drainage-scanning path is reasonable.

Finally, the magnitude of capillary cohesion is highly dependent on the assumed surface tension of water and is suspected of deviating from the assumed value. A Wilhelmy Plate experiment [7] has shown deviations in measured surface tension when deionised water is brought into contact with natural granular material. In addition, when evaluating the capillary cohesion based on Eq. 4, uncertainties from the effective friction angle, which may vary, remain.

Furthermore, the role of interlocking effects in the volume change behaviour during uniaxial compression cannot be considered but may influence the determined capillary cohesion in uniaxial compression experiments.

5 Conclusion and Outlook

By systematically testing specimens at varying degrees of saturation in uniaxial compression experiments, we determined the dependency of capillary cohesion on the degree of saturation, which is in good agreement with the theoretical considerations made by [14]. In addition, we computed the theoretical capillary cohesion derived from cyclic water retention curves, which showed a fair match to the result from uniaxial compression experiments but diverged slightly in magnitude. By connecting the results from macroscopic experiments to insights from CT data, we established a link between micromechanical properties and macroscopic soil behaviour.

There is a fair match between capillary cohesion determined in macroscopic uniaxial compression experiments and theoretical capillary cohesion based on the WRC and the one derived from CT images. The similar order of magnitude justifies further investigations. Future evaluations of image data from uniaxial compression tests seem promising, extending the work done by [16] is still under progress. This fundamental research, examining capillary cohesion of granular soils, with the help of tomographic image data, will help to gain a better understanding of the interaction between water, air, and the grain skeleton.

This work is funded by the German Research Foundation (Deutsche Forschungsgemeinschaft, DFG) in the framework of Research Training Group GRK 2462: "Processes in natural and technical Particle-Fluid-Systems" at Hamburg University of Technology (TUHH) and DFG project 401096010 "Microscale investigations of the hydro-mechanical behaviour of unsaturated granular soils with computed tomography."

References

[1] N. Lu, W. J. Likos, J. Geotech. Geoenvironmental Eng. **132**, 2 (2006)
[2] D. G. Fredlund, H. Rahardjo, M. D. Fredlund, *Unsaturated soil mechanics in engineering practice,* Wiley (2012)
[3] N. Lu, J. W. Godt, D. T. Wu, Water Resour. Res. **46**, 5 (2010)
[4] W. G. Gray, B. A. Schrefler, and F. Pesavento, J. Mech. Phys. Solids **57**, 3 (2009)
[5] E. Nikooee, G. Habibagahi, S. M. Hassanizadeh, and A. Ghahramani, Transp. Porous Media **96** (2013)
[6] J. Wang, P. Lambert, T. De Kock, V. Cnudde, B. François, Acta Geotech. **14** (2019)
[7] M.Milatz, Habilitation thesis, TUHH Open Research (TORE), DOI: 10.15480/882.4803 (2022)
[8] M. Milatz, E. Andò, G. Viggiani, S. Mora, Open Geomech. **3**, 5 (2022)
[9] D. Heinrich, M. Milatz, Proc. of ICPMG 2022 (2022)
[10] M. Milatz, E3S Web of Conferences **195** (2020)
[11] D. Heinrich, M. Milatz, TUHH Open Research (TORE), DOI: 10.15480/336.4393 (2022)
[12] M. Milatz, Acta Geotech. **15**, 8 (2020)
[13] D. Heinrich, M. Milatz, TUHH Open Research (TORE), DOI: 10.15480/336.4394 (2022)
[14] H. Schubert, Chem. Ing. Tech. **45**, 6 (1973)
[15] Deutsche Gesellschaft für Geotechnik e. V., *Empfehlungen des Arbeitskreises "Baugruben", (EAB)*, Ernst & Sohn (2017)
[16] M. Milatz, N. Hüsener, E. Andò, G. Viggiani, J. Grabe, Acta Geotech. **16**, 11 (2021)